World Academy of Science, Engineering and Technology
International Journal of Mechanical and Mechatronics Engineering
Vol:6, No:6, 2012

Study on the Deformation Modes of an Axially Crushed Compact Impact Absorption Member

Shigeyuki Haruyama, Hiroyuki Tanaka, Dai-Heng Chen, Aidil Khaidir Bin Muhamad

***Abstract*—**In this paper, the deformation modes of a compact impact absorption member subjected to axial compression are investigated using finite element method and experiments. A multiple combination compact impact absorption member, referred to as a 'compress-expand member', is proposed to substitute the conventional thin-walled circular tube. This study found that the proposed compact impact absorption member has stable load increase characteristics and a wider range of high load efficiency (P_{ave}/P_{max}) than the thin-walled circular tube. Moreover, the proposed compact impact absorption member can absorb larger loads in a smaller radius than the thin-walled cylindrical tube, as it can maintain its stable deformation in increased wall thicknesses.

***Keywords*—**axial collapse, compact impact absorption member, finite element method, thin-walled cylindrical tube.

I. Introduction

IN today's automotive industries, lightweight cars with robust designs and crash-resistant structures have attracted significant attention and market potential. This is mainly attributed to the increasing awareness of passenger safety among consumers, and the economic and environmental values associated with these cars. However, to develop vehicles with a combination of weight reduction and safety improvement is a complicated task. Weight reduction can only be achieved through limiting the use of materials or through using alternative materials, which affects the structure rigidity. However, a strong and rigid structure is essential to prevent the over-deformation that can harm passengers during collisions. This study has considered the use of components that are lightweight, yet capable of controlling deformation. It has also considered the magnitude of the impact force of collisions, and the direction of the impact, in relation to the materials used.

Impact absorption members are often used in vehicles to protect passengers and the car structure during collisions. They are mainly placed at the front and rear of the car body to function as axial energy absorption mechanisms. Until recently, various thin-walled tubular members—such as cylindrical tubes, square tubes, cylindrical tubes with corrugated surfaces, and hexagonal thin-walled tubes with partition plates—have been proposed as the impact absorption members, and their properties and crushing behaviours have been investigated [1]–[12]. TABLE I (a) and (b) show each tubular member and its properties when subjected to axial crushing.

For cylindrical tubes, as stated by Alexander [1], energy is absorbed by strain from the continuous bending and expanding deformation of the plastic hinge of folds that are formed during the axial crushing process. During this process, high first peak load and load fluctuations with large amplitudes occur in the load-deformation relationship that corresponds to the bellow-shaped deformation caused by the continuous fold formation. The fluctuation of the load affects the capability of the cylindrical tubes, as it reduces their energy absorption efficiency. Most cylindrical or square tubes have difficulty withstanding large loads because of their small diameter. Reducing the radius would cause the bend to collapse, while increasing the thickness would make the formation of local folds harder.

Chen *et al.* [8] conducted a study on the axial crushing properties of cylindrical tubes with a corrugated surface. In this study, it was found that two different deformation modes can be obtained from the crushing process. These were labelled P-mode and S-mode. In P-mode, compressive load fluctuated according to the continuous fold formation. However, unlike cylindrical tubes, it had smaller load amplitude and a smaller gap between first peak load and average load. In contrast, in S-mode, regardless of the fold formation, compressive force increased uniformly. The absence of load fluctuation during the deformation made the S-mode tube preferable as the impact absorption member because the stable, monotonous load increase creates higher energy absorption efficiency. However, as shown in Fig. 1, there are size limitations for corrugated surface cylindrical tubes to deform as S-mode. Moreover, their energy absorption volumes were lower when compared to the cylindrical tube.

Following this, Chen *et al.* [12] conducted a new study on the crushing behaviour of hexagonal thin-walled tubes with partition plates. They discovered that this also had small load amplitude. However, this time, a broader peak-average load gap was obtained.

Overall, these examples illustrate tubular members that use buckling as their measure of deformation and absorption of impact energy. Many problems related to buckling—such as instability, presence of load fluctuation and poor efficiency in energy absorption—have affected the performance of these tubular members and their feasibility as practical impact

S. Haruyama is with the Yamaguchi University Graduate School of Innovation and Technology Management, Tokiwadai 2-16-1, Ube, Yamaguchi, 755-8611 Japan (e-mail: haruyama@yamaguchi-u.ac.jp).

H. Tanaka is with the Kyushu Institute of Technology, Sensuicho 1-1, Tobata-ku, Kitakyushu-shi, 804-8550 Japan.

D. Chen is with the Tokyo University of Science, Faculty of Engineering, Kudankita 1-4-16, Chiyoda-ku, Tokyo, 102-0073, Japan.

A.K. Bin Muhamad is with the Yamaguchi University, Faculty of Engineering, Department of Mechanical Engineering, Tokiwadai 2-16-1, Ube, Yamaguchi, 755-8611 Japan.

absorption members.

Therefore, this study proposes a multiple combination impact absorption member, as shown in Fig. 2 (referred to in this paper as a 'compress-expand member'). This uses compression and expansion as its energy absorption mechanism. Compared to thin-walled cylindrical tubes, this compact impact absorption member can absorb larger loads in a smaller radius, and has higher energy absorption efficiency. In this study, the proposed compact impact absorption member's deformation properties were investigated through an axial crushing experiment and crushing simulation by using finite element method (FEM). Following this, the deformation properties were evaluated using an approximate equation.

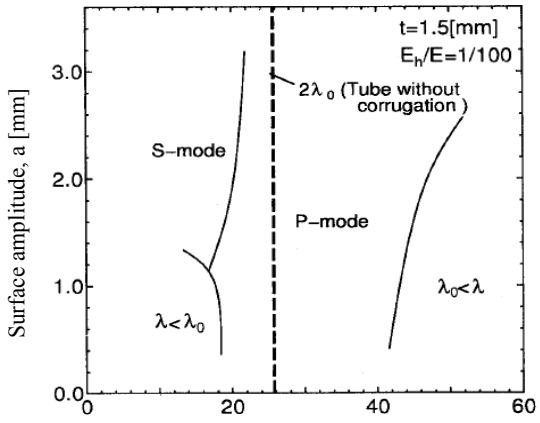

Fig. 1 Modes classification chart for cylindrical tubes with corrugated surface, by Chen *et al.* [8]

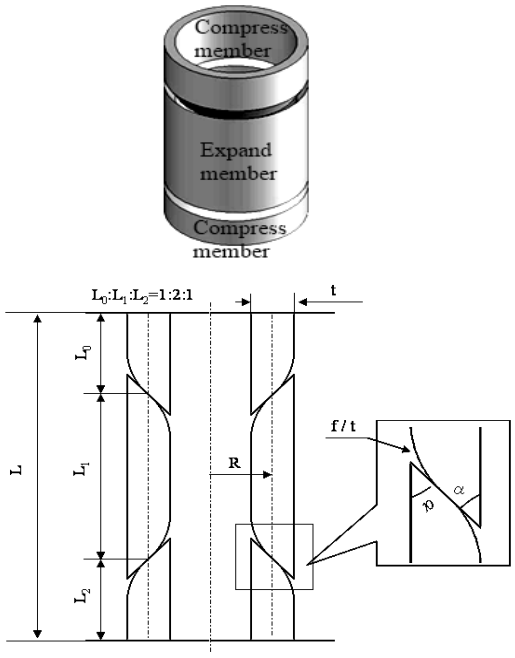

Fig. 2 Compress-expand member

TABLE I (A)
TUBULAR MEMBERS AND THEIR PROPERTIES

Before deformation	After deformation
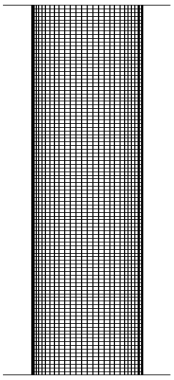 Cylindrical tubes	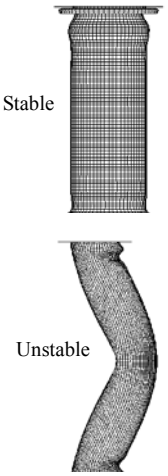 Stable Unstable
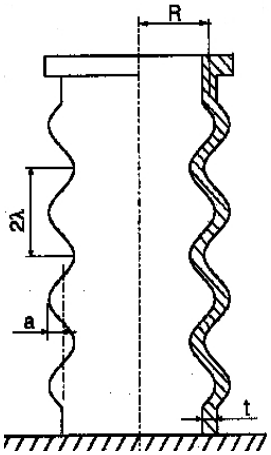 Cylindrical tubes with corrugated surfaces	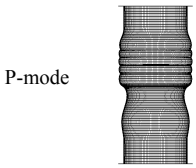 P-mode 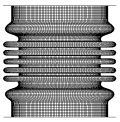 S-mode
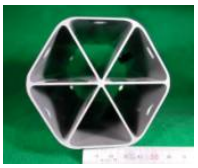 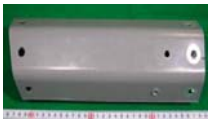 Hexagonal thin-walled tubes with partition plates	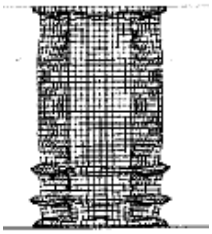

2λ = surface wavelength [mm]
a = surface amplitude [mm]
t = thickness [mm]
R = radius [mm]

TABLE I (B)
TUBULAR MEMBERS AND THEIR PROPERTIES

Type	Load-displacement curve
Cylindrical tubes	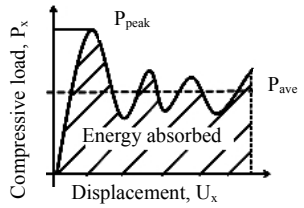
Cylindrical tubes with corrugated surfaces	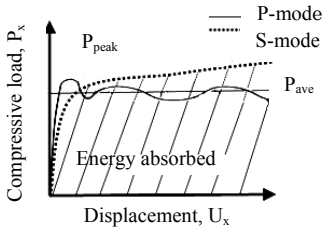
Hexagonal thin-walled tubes with partition plates	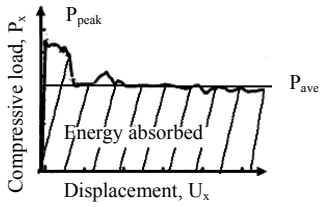

II. INVESTIGATIONS ON COMPRESS-EXPAND MEMBER

A. Experiment Materials and Specimens Dimension

The material used in this study was a general structure rolled steel. To determine its mechanical properties, a JIS4 test specimen of the material was fabricated and a tensile test was conducted. This tensile test used a tensile test machine with a displacement gauge (DVE-200S non-contact video extensometer gauge), which was installed to Shimadzu Corp. Autograph (AG-10T). The load-displacement relationship of the materials was measured during the tensile test using a memory recorder analyser (EDX-1500A Kyowa Electronic Instruments), with the sampling rate set to 100[Hz]. The result was then used to determine the nominal stress-strain curve of the material.

Fig. 3 (a) and (b) show compress-expand members one and two, which consisted of two combined parts (penetrating member and expanding member, wall thickness 2.5[mm], taper angle 2[deg]). Fig. 3 (c) shows the compress-expand member three, which consisted of three separated parts (two parts compress-penetrating member and one part expanding member). An axial compression test was conducted on each compress-expand member. All components were produced using NC lathe cutting.

B. Actual Evaluated Experiment

The test equipment used in the axial crushing experiment was the Shimadzu Hydraulic Control 200t Universal Testing Machine, equipped with a SUNX Laser Displacement Sensor. Load and displacement data were read using a memory recorder analyser (EDX-1500, Kyowa Electronic Instruments Co. Ltd.). Data was collected through the sampling speed of 100[Hz] and plotted as a load-displacement curve. Then, with the crushing speed set to 40[mm/min], deformation of the test specimen was captured using a digital video camera (frame rate 30[fps]). This measurement was synchronised with the memory recorder analyser. To mount the test specimen without applying a forced fixture on the top and bottom surfaces, the degree of adhesion for both surfaces was increased by coating with a lubricant.

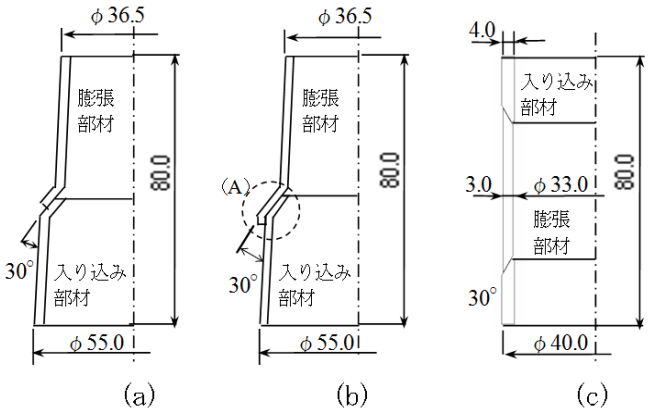

Fig. 3 Tube geometry and loading condition

C. Experiment Results and the Investigation

Fig. 4 shows the relationship of axial load, P_x, and displacement, U_x, for compress-expand members one and two obtained from the experiment. Fig. 5 (a) and (b) and Fig. 6 (a')–(c') show the deformed shape of point (a) and (b) and (a')–(c') on Fig. 4. Similarly, Fig. 7 shows the relationship of load and displacement for compress-expand member three,

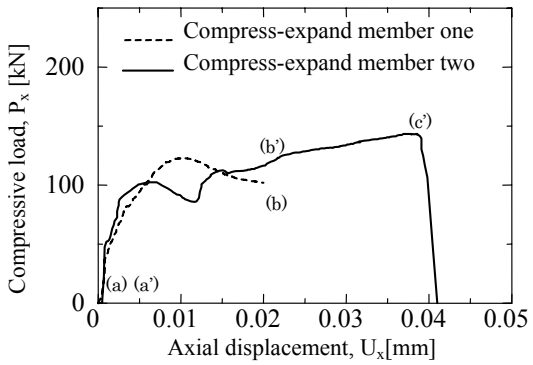

Fig. 4 Load-displacement curve for compress-expand members one and two

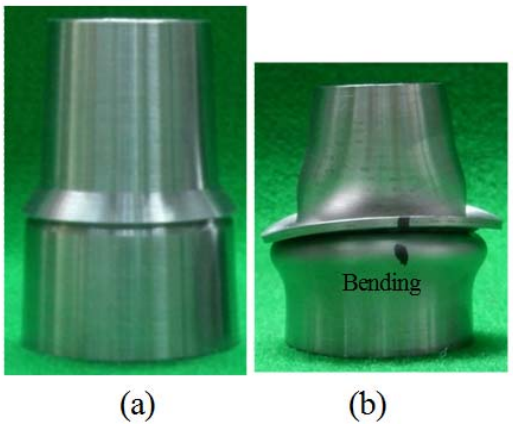

Fig. 5 Deformation of compress-expand member one

while Fig. 8 shows its deformed shape as obtained from the actual experiment and FEM analysis. The details of the analysis method will be explained in Section III. For compress-expand member one, as shown in Fig. 5 (a), due to the insufficient penetration of the penetrating member into the expanding member during the axial compression process, local bending occurred at the point of contact of both members. As a result, the expansion deformation failed to take place.

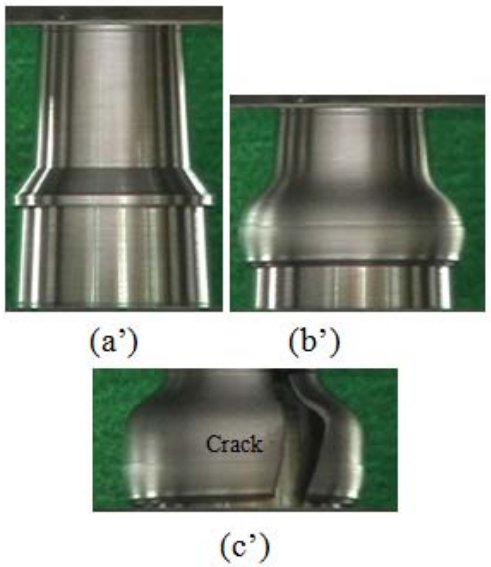

Fig. 6 Deformation of compress-expand member two

Therefore, the test was cancelled mid-way. For compress-expand member two, to stabilise the penetration process, the point of contact of the expanding member and penetrating member was designed with a more elongated shape, as shown by part (A) of Fig. 3 (b). As a result, the penetration and expansion deformation shown in Fig. 6 (b') was obtained. Here, as shown by Fig. 6 (c'), during compression, the increase in circumferential strain during the expansion process caused an axial crack to occur on the expanding member's surface. The compression load, P_x, decreased rapidly as the crack formed.

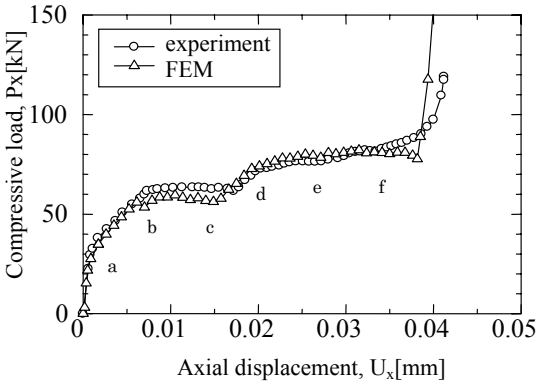

Fig. 7 Load-displacement curve for compress-expand member three (exp. and FEM)

This phenomenon demonstrated the importance of evaluating the contact condition of the penetrating part and the strain produced during expansion deformation. Following this, the load of the axial compression of compress-expand member three, from its load, P_x, to displacement, U_x, curve (Fig. 7) and deformation process (Fig. 8 (a)~(f)), showed a rapid increase during the movement of the penetrating member into the expanding member. As the continuous expansion deformation took place, a monotonous load with stable load-displacement relationship was obtained.

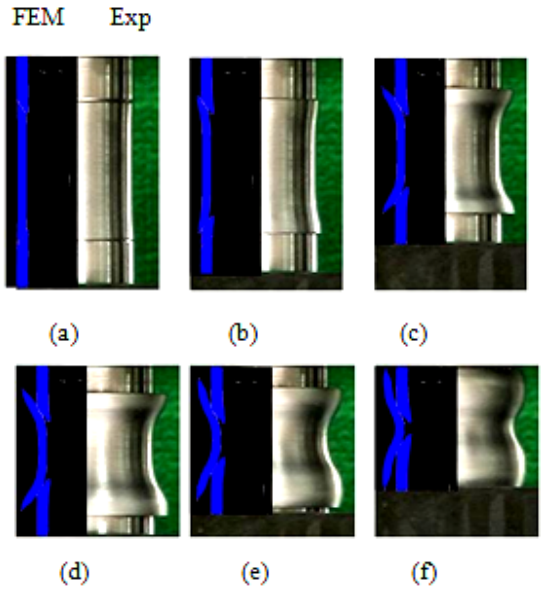

Fig. 8 Deformation of compress-expand member three (exp. and FEM)

As the compression process progressed, the penetrating member from both sides piled up and caused the load to increase abruptly. As shown in Fig. 8, the deformation diagram for compress-expand member three showed strong

agreement between the actual experiment and FEM. Regarding this, in this study, investigation of the impact absorption properties of compress-expand member three when applied with axial compression load was conducted using numerical analysis of FEM. In particular, this study sought to propose an evaluation method based on the approximation formula of the energy absorption amount, which was important for designing the impact absorption member.

III. Analysis Method

This study conducted elastic-plastic large deformation analysis using FEM general purpose analysis software, MSC.Marc, upon the axial crushing deformation of the compress-expand member shown in Fig. 9 (length, L; thickness, t_0, t_1; mean radius, R_0, R_1; contact angle, α) to investigate the contact condition of penetrating member (contact angle), circumference strain for crack prediction, and energy absorption characteristics. The analysis used an isoparametric quadrilateral arbitrary four-node axisymmetric solid element to model the shape of the compact impact absorption member. The element in the axial and thickness direction was divided to be approximately square shaped. The material was assumed to have the properties of steel and isotropic bodies that obey von Mises's yield criterion. The relationship between stress, σ, and strain, ε, in the uniaxial stress state of the material during the post-yield period was

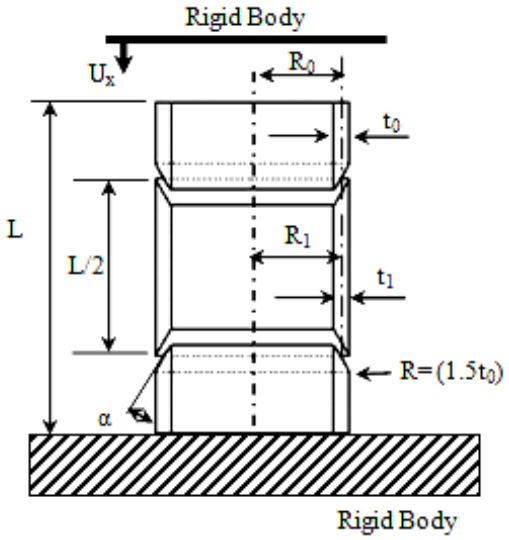

Fig. 9 Tube geometry and loading condition fixed to a rigid body

represented using bilinear hardening law, as shown by (1). Yield stress, σ_y, was a function of initial yield stress, σ_y = 206MPa; equivalent plastic strain; work hardening coefficient, E_h (E_h/E=1/100); Young's modulus, E = 206[GPa]; and Poisson's ratio, ν = 0.3. For boundary condition, as shown in Fig. 9, the member's bottom section was fixed to a rigid surface, while, the top—another rigid surface defined with displacement control in axial direction (X direction)—compressed the member. In this case, the coefficient of friction was not considered. Glue function was used to make the surface rigid, and the member's top side was fully restrained during the moment of contact. The elastic-plastic large deformation analysis conducted in this study used von Mises's yield criterion as the plastic yield condition, Updated Lagrangrian Formula for the formulation of nonlinear deformation behaviour, and Newton-Rahpson Method for the solution of nonlinear equations.

$$\sigma_y = \sigma_0 + E_h\left(\varepsilon - \frac{\sigma_0}{E}\right) \quad (1)$$

IV. Analysis Results and Investigation

A. Investigations on Load Efficiency

To comprehend the energy absorption properties of the proposed compress-expand member, theoretical analysis using FEM of the member dimension and energy absorption efficiency was conducted. The energy absorption efficiency was the product of the average load and maximum load ratio (P_{ave}/P_{max}). Fig. 10 shows the load-displacement relation for the compress-expand member with radius, R = 10[mm], and thickness, t = 3[mm], while L is changed from 60[mm] to

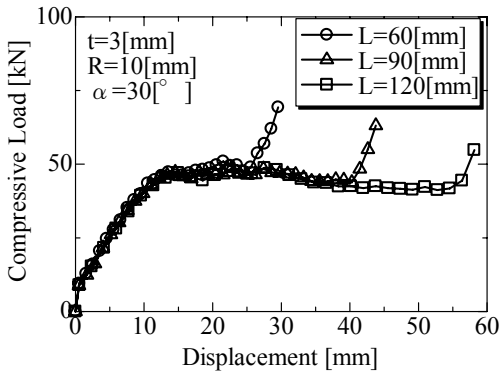

Fig. 10 Load-displacement curve for varied lengths

90[mm] to 120[mm]. Fig. 11 shows the deformation process of the L = 120[mm] member. From both figures, during the initial penetration (see Fig. 11, 10[mm]), a uniform load increase could be seen on the load-displacement curve. As the continuous expanding deformation took place (see Fig. 11, 20–50[mm]), a stable, constant load with small amplitude was obtained. Further compression caused the penetrating member and expanding member to pile up, which made the penetrating member contact both sides and caused a rapid load increase. As shown in Fig. 10, from displacement 20[mm] to 50[mm], the constant load part was gradual. However, as the deformation progressed, the load slightly decreased. This can be explained with the deformation diagram shown in Fig. 11. When the thicknesses of both the expanding member and compressing (penetrating) member were equal, the tips of both penetrating members deflected into the radial direction as the deformation progressed. This caused the tip of the penetrating member and the wall of the expanding member to disengage

slightly, thus reducing the reaction force that opposed the compressive load applied. As length, L, changed from 60[mm] to 90[mm] to 120[mm], the load-displacements showed an approximately uniform pattern. Therefore, the load-displacement property of the proposed compress-expand member was not affected by the change in length. The relationship between load efficiency and thickness-radius ratio, t/R, for length-thickness ratio, L/t, of 20, 30, 40 and 60 is presented in Fig. 12. The results show that, at the larger t/R, load efficiency became high when the L/t ratio was increased. This could be due to the influence of the initial rising load, which increased as the member's length decreased.

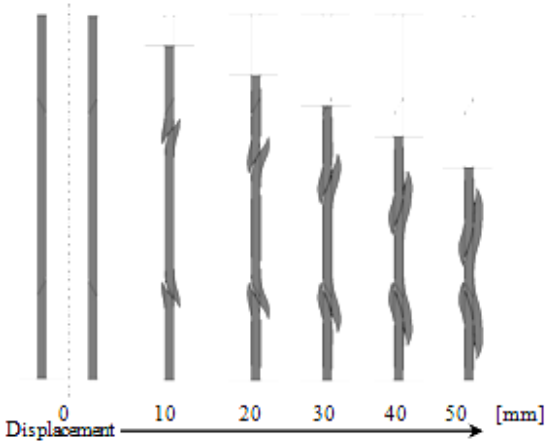

Fig. 11 Deformation diagram (R=10[mm], L=120[mm], t=3[mm])

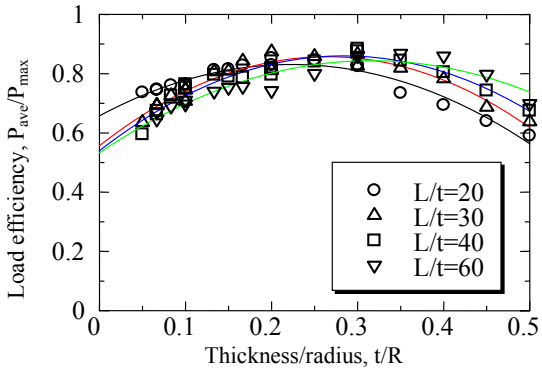

Fig. 12 Load efficiency versus t/R

B. Investigation of the Load Efficiency of Cylindrical Tubes and Compress-Expand Members

To conduct an investigation of the load efficiency comparison between cylindrical tubes and compress-expand members, the radius and length for both components were set to be equal, where R = 20[mm] and L/t = 20. Fig. 13 shows the analysis results presented in the form of load efficiency versus thickness-radius ratio, t/R, where thickness, t, was the manipulated parameter. As shown in Fig. 13, for cylindrical tubes, load efficiency peaked at t/R = 0.1(a relatively thin wall thickness). However, the load efficiency significantly fell as the thickness increased. On the other hand, the compress-expand members showed high load efficiency at the t/R = 0.15–0.30 range. The load efficiency declination was also smaller when compared to the cylindrical tubes. Concerning this, axial crushing analysis was conducted on a cylindrical tube with geometry dimension, t/R = 0.1, and a compress-expand member with geometry dimension, t/R = 0.3. These were the dimensions when the load efficiencies were at peak. The compression load–circumferential strain curve

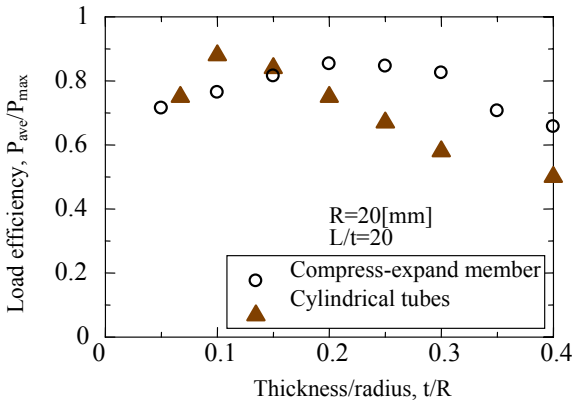

Fig. 13 Load efficiency for compress-expand member and circular tube

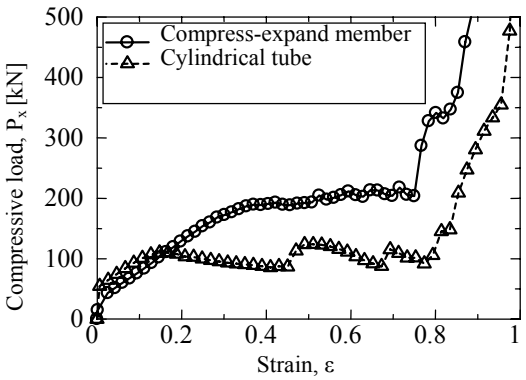

Fig. 14 Load comparison between compress-expand member and circular tube

obtained from the analysis is shown in Fig. 14. From Fig. 13 and Fig. 14, it can be seen that compress-expand members withstand larger load while under the same strain, and have better load efficiency in larger t/R when compared to cylindrical tubes. This means that the wall thickness of the compress-expand member can be expanded even in a small radius. Therefore, it is possible for the compress-expand members to receive larger load and have higher load efficiency in a more compact size than cylindrical tubes. However, as the compress-expand members were in the range where t/R was over 0.4, it was discovered that a local buckling occurred near the contact area of the compression (penetrating) member's body.

C. Contact Angle Influence on Buckling

Fig. 15 shows the presence of buckling during axial crushing when the contact angle, α, of the penetrating member and expanding member was changed from 30[deg] to 45[deg], 60[deg] and 75[deg]. In the analysis, the effect of friction was neglected and the result was plotted as thickness over radius ratio, t/R, against length over thickness ratio, L/t. Buckling occurrence in every contact angle is denoted by 'stable' (buckling free) and 'unstable' (buckling occurred). For the contact angles 60[deg] and 75[deg], buckling occurred at t/R over 0.3, while for the contact angles 30[deg] and 45[deg], buckling occurred at t/R over 0.4. Change in L/t value had no effect on buckling occurrence. Buckling was detected near the region of contact between the rigid body and the compress-expand member. From the results obtained, it is understood that the contact angle designed must be below 45[deg]. However, in this research, the effect of the friction force was neglected. Therefore, investigations considering friction influence need to be conducted in the future.

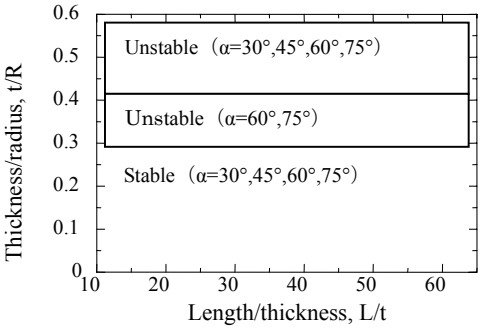

Fig. 15 Deformation modes distribution of contact angles

D. Geometrical Shape Influence on Circumferential Strain

The compress-expand member used the expansion strain that resulted from the difference in the radiuses of the penetrating member and the expanding member to absorb energy. Therefore, it could obtain a high deformation load by increasing the circumferential strain. However, from the results of the crushing test, Fig. 6 (c') shows that cracking can occur as the circumferential strain becomes larger. Therefore, this study undertook an investigation into the relationship between compression load, P_x, and displacement, U_x, in compression analysis for radius difference. As shown in Fig. 16, the compress-expand member dimension was set with wall expansion rate, δ = t, 1.25t, 1.5t_1; radius, R = 10[mm]; thickness, t = 3[mm]; and length, L = 100[mm]. Then, to reduce the effect of penetrating member deflection, the thickness ratio of penetrating member and expanding member was set to 2:1. Fig. 17 shows each geometry's load-displacement curve. From this figure, it can be seen that the increase of compression load was in accordance with the increase in wall expansion rate. This was due to the rise in circumferential strain as the radius difference between the penetrating and expanding members became larger. Therefore, as mentioned above, compress-expand members can obtain higher loads by increasing the radius difference between members; however, in the meantime, circumferential strain also rises. Therefore, to avoid sudden load drops caused by cracking, it was necessary to investigate the evaluation method of the circumferential strain. Using the geometries shown in Fig. 16, an investigation of the evaluation method was performed. The circumferential strain derived from the member's dimension can be represented approximately using (2). Fig. 19 shows the result of maximum circumferential strain obtained from (2), together with circumferential strain from the FEM analysis, $\varepsilon_{\theta max}$, versus the thickness-radius ratio, t/R. Fig. 19 also presents $\varepsilon_{\theta max}$ - t/R relation from the theoretical equation of maximum strain obtained from the

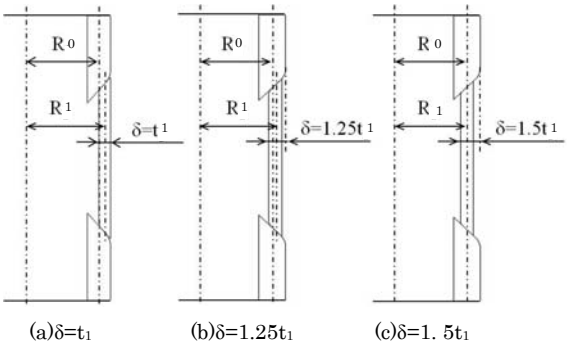

Fig. 16 Compress-expand member with difference in radius for compress member and expand member (t_1=3[mm])

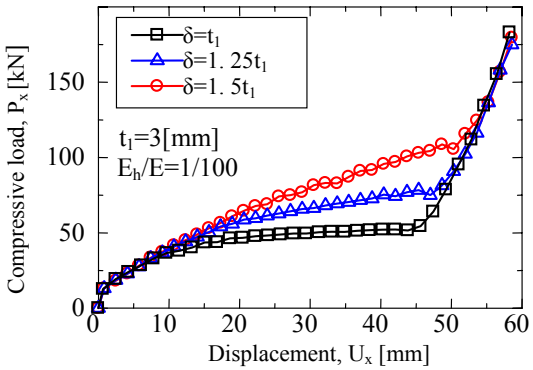

Fig. 17 Load-displacement curve with radius difference

strain concentration of the thin-walled cylindrical tube's local folds [11]. From this figure, it can be seen that both the circumferential strain from the approximate equation and the FEM analysis results were almost uniform. However, at the smaller thickness ratio range (t/R = 0.1–0.15), the results from the FEM analysis became higher, while at the larger thickness ratio range (t/R=0.2–0.3), it became smaller. This is explained in Fig. 18—the deformation diagram for δ = 1.5t_1. Here, the expanding member became larger than the compress member's outer radius, thus causing a slightly larger value than the approximate equation. Furthermore, with the increase of the thickness-radius ratio, in all sizes used in this analysis, the compress (penetrating) member deflected at radius direction when crushed axially, thus producing a smaller circumferential strain. Therefore, in this analysis, it is

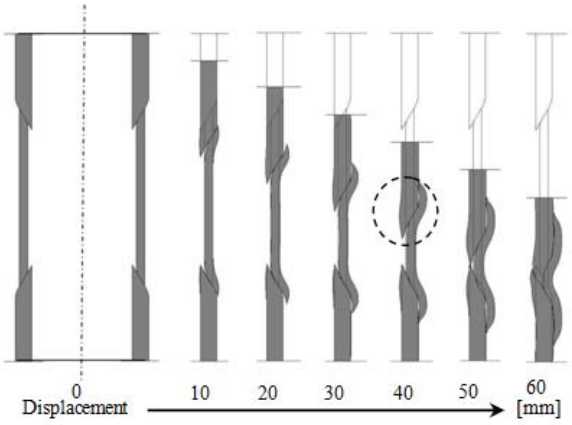

Fig. 18 Deformation diagram (t_2=3[mm], δ=1.5t_2 load)

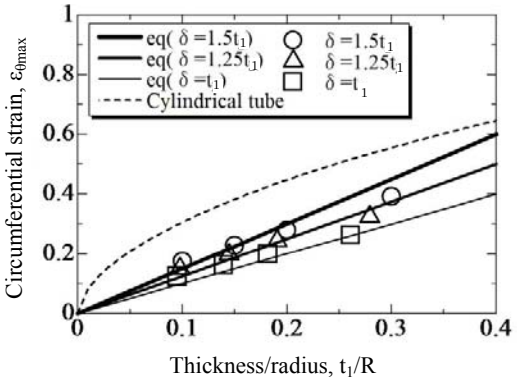

Fig. 19 ε_θ from approximate equation and FEM

understood that circumferential strain can also be varied by the thickness-radius ratio. However, for prediction purposes, the approximate formula used is still considered valid. The next section discusses this study's investigation of average load and crushing rate, which was important when designing the proposed compress-expand member.

$$\varepsilon_\theta \cong \frac{\frac{t_0}{2}+\frac{t_1}{2}-\delta}{R_1} \tag{2}$$

V. Investigations on Approximate Equation

A. Average Load

The compress-expand member began absorbing energy through the deformation when the penetrating tube member entered the expand member. As a result, by using circumferential stress-strain relation, as is shown by (2), it was possible to predict the crushing load approximately. The circumferential strain derived by the different centre radiuses of the compress member and expand member is shown by (2). The average crushing load of the compress-expand member was evaluated approximately by using the member's geometric dimension and stress-strain relation, as shown by (3). Equation (4) was obtained by substituting (2) into (3). Here, $\delta = |\ R_1\text{-}R_0|$ is the difference in the centre radiuses of the expanding member and the penetrating member. For cases in which the thickness of the penetrating member; the thickness of the expanding member, t; and the radius, R, are equal, (5) is obtained. Similarly, if the flow stress, σ_{flow}, as shown in (6), is used, (4) and (5) can be represented as (7) and (8). Maximum crushing rate was determined at the point at which the load began to increase rapidly as the penetrating member and expanding member piled up and contacted at axial direction.

$$P = \frac{\sigma_y \varepsilon_\theta \times 2\pi R_1 t_1 \times L}{L} \tag{3}$$

$$P = \sigma_y \times 2\pi R_1 t_1 \times \left(\frac{t_0/2 + t_1/2 - \delta}{R_1} \right) \tag{4}$$

$$P = 2\pi t^2 \sigma_y \tag{5}$$

$$\sigma_{flow} = \sigma_y + E_h \varepsilon_\theta \tag{6}$$

$$P' = 2\pi t_1 \times \sigma_{flow} \times \left(\frac{t_0}{2} + \frac{t_1}{2} - \delta \right) \tag{7}$$

$$P' = 2\pi t^2 \sigma_{flow} \tag{8}$$

B. Crushing Rate

Crushing rate is represented by δ_{OA}, which is the displacement of the wedge shaped part of the expanding member until its expansion to the penetrating member's outer radius; and δ_{AC}, which is the displacement as members start to overlap when the edge of penetrating members contact each other, resulting in a rapid increase in load. The total crushing rate is represented by the sum of δ_{OA} and δ_{AC}. The crushing rate, δ_{OA} and δ_{AC}, can be derived approximately from the geometric dimension, as shown by (9) and (10). Equation (11) shows the total crushing rate.

$$\delta_{OA} = \frac{2\left(\frac{t_0}{2} + \frac{t_1}{2} - \delta \right)}{\tan\alpha} \tag{9}$$

$$\delta_{AC} = \frac{L}{2} - \frac{2t_0 + t_1}{\tan\alpha} \tag{10}$$

$$\delta_{all} = \frac{L}{2} - \frac{2\left(\frac{t_0}{2} + \delta \right)}{\tan\alpha} \tag{11}$$

C. Approximate Equation and Investigation

To investigate the validity of the proposed approximate equation, a comparison was performed of the approximate equation and the FEM analysis result of the compress-expand member, with the dimensions shown in Fig. 16. Fig. 20 shows the relationship between the average load, P_{ave}; crushing rate, δ_{all}; and thickness ratio, t/R, for each geometry, as obtained from the FEM analysis result and the approximate equation. From the figure, for average load, the value from the FEM analysis result became high at $\delta = t_1$, while at $\delta = 1.5t_1$, the value from the approximate equation became high. This was uniform with the results of circumferential strain denoted in the previous section. Moreover, for crushing rate, there was strong agreement between the value of the FEM analysis result and the approximate equation. Table 1 shows the result

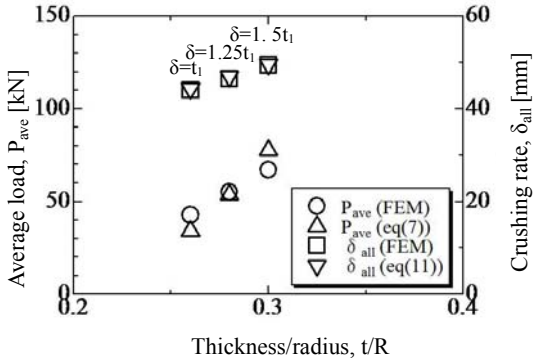

Fig. 20 Average load, P_{ave}, and crushing rate, δ_{all}, from approx. equation and FEM

obtained from the FEM analysis result and the approximate equation for the amount of energy absorption. From the table, it was found that the error of energy absorption amount was below 20 per cent, which is in strong agreement with the approximate equation. Thus, it is valid to use these as the prediction formula for the design.

TABLE II
COMPARISON OF ENERGY ABSORPTION AMOUNT (APPROX. EQUATION, FEM)

			AMOUNT OF ENERGY ABSORPTION	
δ	t/R	R	FEM (KJ)	Eq (KJ)
t_1	0.26	11.5	1.88	1.51
$1.25t_1$	0.28	10.75	2.56	2.52
$1.5t_1$	0.30	10.0	3.32	3.85

VI. CONCLUSION

In this study, axial compression tests of actual specimens, theoretical analyses by FEM, and investigations of approximate equation were performed on the proposed compress-expand member. Regarding the impact absorption properties of the compress-expand member, the following conclusions were reached:

(1) A small load amplitude, monotonous load increase and stable load-displacement relationship were obtained in the axial crushing of the compress-expand member.
(2) Compared with the cylindrical tube, the compress-expand member had a high load efficiency in the smaller radius, even if the member's wall was thicker. Furthermore, a high axial crushing load could be absorbed by increasing the radius difference between the expanding member and the compress (penetrating) member.
(3) Buckling occurred on the penetrating member when the contact angle between the compress member and expand member was increased. In addition, the probability of buckling occurrence became high with the increase in thickness-radius ratio.
(4) The circumferential strain of the compress-expand member can be approximately predicted using (2). Circumferential strain increased proportionally with the increase in thickness ratio, t/R.
(5) The average load and crushing rate of the compress-expand member can be approximately estimated using (7) and (11).

ACKNOWLEDGMENTS

The fourth writer wishes to thank his supervisor and fellow colleagues at Strength of Materials Laboratory, Department of Mechanical Engineering, Faculty of Engineering, Yamaguchi University, Japan for their cooperation and support.

REFERENCES

[1] J. M. Alexander, "An approximate analysis of the collapse of thin cylindrical shells under axial loading," *Quarterly Journal of Mechanics and Applied Mathematics*, 13–1, pp. 10–15, 1960.
[2] T. Wierzbicki, S. U. Bhat, W. Abramowicz and D. Brodkin, "Alexander revisited—a two folding elements model of progressive crushing of tubes," *International Journal of Solids and Structures*, 29–24, pp. 3269–3288, 1992.
[3] W. Abramowicz and N. Jones, "Dynamic progressive buckling of circular and square tubes," *International Journal of Impact Engineering*, 4–4, pp. 243–270, 1986.
[4] W. Abramowicz and N. Jones, "Dynamic axial crushing of circular tubes," *International Journal of Impact Engineering*, 2–3, pp. 263–281, 1984.
[5] T Wierbicki, S. U. Bhat, W. Abramowicz and D. Brodkin, "Alexander revisited—a two folding elements model of progressive crushing of tubes," *International Journal of Solids and Structures*, 29–24, pp. 3289–3295, 1992.
[6] K. Ushijima, S. Haruyama, H. Hanawa and D. Chen, "Strain concentration for cylindrical tubes subjected to axial compression," *Transactions of the Japan Society of Mechanical Engineers* (in Japanese), vol. 71, no.707, pp. 1023–1029, 2005.
[7] D. Chen and K. Masuda, "Deformation modes for axial crushing of cylindrical tubes considered of the edge effect," *Transactions of the Japan Society of Mechanical Engineers* (in Japanese), vol. 73, no. 773, pp. 1029–1036, 2007.
[8] T. Hiratsuka, D. Chen and K. Ushijima, "Axially compression of corrugated cylinder," *The Society of Automotive Engineers of Japan*, paper no. 20055304.
[9] D. Chen and T. Hiratsuka, "Study of axially crushed cylindrical tubes with corrugated surface based on numerical analysis," *Transactions of the Japan Society of Mechanical Engineers* (in Japanese), vol. 72, no. 722, pp. 1464–1471, 2006.
[10] K. Ushijima *et al*., "Study on axially crushed cylindrical tubes with grooved surface," *Transactions of the Japan Society of Mechanical Engineers* (in Japanese), vol. 71, no. 707, pp. 1015–1022, 2005.
[11] K. Ushijima *et al*., "Strain concentration for cylindrical tubes subjected to axial compression," *Transactions of the Japan Society of Mechanical Engineers* (in Japanese), vol. 71, no. 707, pp. 1023–1029, 2005.
[12] D. Chen *et al*., "Crushing behaviour of hexagonal thin-walled tube with partition plates," *Transactions of the Japan Society of Mechanical Engineers* (in Japanese), vol. 72, no. 724, pp. 1978–1984, 2006.